Ceramics-Silikáty 64 (4), 434-446 (2020)
www.ceramics-silikaty.cz doi: 10.13168/cs.2020.0031

USE OF PARTIALLY HYDROLYZED PVA FOR BORON CARBIDE SYNTHESIS FROM POLYMERIC PRECURSOR

OGUZ KARAAHMET, #BUGRA CICEK

Yıldız Technical University, Department of Metallurgical and Materials Engineering, 34210, Esenler, Istanbul, Turkey

#E-mail: bugracicek@gmail.com

Submitted April 24, 2020; accepted June 8, 2020

Keywords: Industrial raw materials, Sol-gel, pH, Composition ratio, Single-source reactant, Low temperature, Boron Carbide (B_4C), Hydrolyzed PVA

Boron carbide (B_4C) synthesis from a polymeric precursor is an alternative to a traditional carbothermal reduction, promising low energy consumption and production costs, particularly for a polymeric precursor such as polyvinyl borate (PVBO). The sol-gel technique is preferred in the production of polymeric precursors owing to its convenience in producing single-source reactants for synthesizing B_4C at low temperatures (< 1800 °C). The sol-gel parameters, such as the composition, viscosity, and pH, affect the formation of the polymeric precursor. In this study, industrial-grade partially hydrolyzed PVA and technical-grade boric acid (H_3BO_3) are used to produce PVBO. We aim to specify the viscosity and pH values for different ratios of PVA:H_3BO_3. A sample with a weight ratio of PVA:H3BO3 of 1:1 (PHD101) is determined to have the optimum process parameters. Calcination is performed between 500 °C and 700 °C for 1-3 h to produce a single-source reactant, which consists of boron oxide (B_2O_3) and carbon. It was observed that B_2O_3 was distributed on the nano-scale level in the carbon matrix. The reactant is heat-treated at 1400 °C for 5 h and crystalline, polyhedral, and irregular B4C particles are synthesized at low temperatures from industrial grade raw materials.

INTRODUCTION

Boron carbide (B_4C) is among the most preferred ceramic materials for defense, abrasion, and nuclear applications. It is a highly effective armor material owing to its engineering properties, such as hardness (HV = 29.1 GPa), density (d = 2.52 g·cm^{-3}), and abrasion resistance [1-3]. Specifically, it is the one of the hardest materials, and it is the hardest material at temperatures exceeding 1100 °C. The nuclear absorption capability of the ^{10}B isotope (at a cross section of 400 - 750 b) has led to the use of B_4C in control rods, neutron shields, and detectors in nuclear reactors [1-7]. Furthermore, B_4C is a chemically inert material and has an acceptable oxidation resistance below 1000 °C, enabling its use as a coating material [2, 5, 8, 9]. However, it has inferior fracture toughness (3.7 MPa·√m) [10]. On the other hand, its lower diffusion coefficient and strong covalent bonding structure limits the sinterability of B_4C [11-13]. Therefore, it is crucial to densify the B_4C powder at elevated sintering temperatures (> 2000 °C) using a hot-press and pressureless sintering to achieve the maximum theoretical density and superior mechanical properties of the resulting B_4C ceramics [2, 4, 14].

Boron carbide can be synthesized using existing methods, including a carbothermal reduction, magnesiothermic reduction, chemical vapor deposition, synthesis from elements, solvothermal reductions, and synthesis from polymeric precursors [2, 4, 15-23]. A conventional carbothermal reduction method is commonly used in commercial electric arc-furnace systems [24]. However, this method is extremely expensive and ineffective for the production of B_4C owing to its high production temperature (> 2000 °C), difficult-to-control stoichiometry, free remaining carbon, necessary finishing processes (such as grinding and leaching to resolve contamination), and long processing time [2, 4, 23-25, 26]. Other synthesis methods, such as a magnesiothermic reduction and chemical vapor deposition, are not cost-effective at an industrial scale. For these reasons, B_4C synthesis using a polymeric precursor has emerged as an alternative method to a carbothermal reduction because a polymer has a convenient controlled composition ratio for use in ceramics, a facile formation, and decomposed at low temperature [22]. Both synthesis methods can use similar boron sources, such as boric acid (H_3BO_3) and boron oxide (B_2O_3). However, the carbon sources differ from those used in the carbothermal method. Boron carbide synthesis with a polymeric precursor uses polyol materials, such as polyvinyl alcohol (PVA), citric acid, glycerol, phenolic resin, and saccharides [22, 27-31]. These chemicals are organic compounds in which the C–O–H bonds have a branched chemical structure. The boron and carbon sources are mixed homogeneously

through a dehydration–condensation reaction from the polyol materials and H_3BO_3, and the surface area of the reactants is increased [32-36]. In addition, B–O–C borate ester bonds in a cross-linking structure are achieved during the dehydration–condensation reaction and yield polyvinyl borate (PVBO) as a polymeric precursor. Pyrolysis or calcination is then applied within the range of 400 °C to 800 °C. Borate ester bonds are destroyed through heat treatment and form a structure with B_2O_3 distributed in the C matrix [28]. Thus, a single-source raw material or reactant can be used to synthesize B_4C at low temperatures (< 1800 °C). The aim of the precursor synthesis from polymeric materials and boron resources is to mix the reactants at molecular levels. A homogenous and uniform reactant distribution during B_4C synthesis leads to an extended intersurface contact between boron and carbon atoms [37], shortening the necessary diffusion route and decreasing the energy of diffusion activation, thereby facilitating the diffusion among the atoms [28]. The structure obtained during the pyrolysis step decreases the thermodynamically and kinetically necessary B_4C synthesis temperatures above 2000 °C and reduces the reaction time [28, 38]. By contrast, residual free carbon in the structure of B_4C materials is the main problem for polymeric precursor synthesis methods [34]. This problem can be solved by optimizing the PVA:H_3BO_3 and C:B_2O_3 ratios and applying thermal decomposition in air [27, 31, 34, 35, 38].

The sol-gel method was used to synthesize the polymeric precursor and determine the physical properties of the end products formed through the following processing. The sol-gel process parameters were affected by the properties of the raw materials, structure of the reactant, and properties of the B_4C. Sol-gel parameters, such as the solubility, viscosity, and pH, vary with the molecular weight, degree of polymerization, and degree of hydrolysis of the PVA, as well as the concentration ratio of the raw materials. Few data are available in the literature regarding the sol-gel process parameters and the effect of the properties of the raw materials applied. In general, the effect of the concentration ratio has been investigated from the composition of the fully hydrolyzed PVA, and the crystalline B_4C powder synthesized at low temperature (1200 - 1500 °C) [27, 28, 38]. The viscosity of the PVA–water and H_3BO_3–water solutions was affected by the polymeric precursor's structure. The water evaporates due to the temperature, and thus the viscosity of the solution increases. Lower viscosity could allow an improved dispersion of boron and carbon in the solution. Thus, the gel was collected a few times to obtain a lower viscosity [37]. However, no detailed information regarding this is yet available in the literature so far. The pH is critical to the particle size and solution during the sol-gel processes [39]. If the pH of the solution is less than 5, the viscosity can decrease and the activation between particles can increase. Conversely, if the pH of the solution increases, the viscosity decreases and a homogeneous solution cannot be obtained [35, 39]. Highly hydrolyzed PVA has been used in previous studies, although few articles have been published regarding B_4C synthesis from partially hydrolyzed PVA–H_3BO_3 [29]. In this study, we used partially hydrolyzed (88 %) and low-molecular-weight (19000-24015) PVA and technical-grade H_3BO_3 as the raw materials to synthesize PVBO and to investigate the effect of the initial concentration ratio on the solution viscosity and pH. As a result, B_4C could be synthesized from the PVBO.

EXPERIMENTAL

Materials

The materials used were boric acid (H_3BO_3, 99.92 %, < 450 μm), polyvinyl alcohol (PVA, degree of hydrolysis of 88, ≤ 5.0 % volatile contents, < 800 μm), and distilled water. Raw materials were used as the starting compounds.

Synthesis of PVBO materials

The synthesis of PVBO was achieved using a dehydration-condensation reaction of PVA and H_3BO_3. First, PVA (1.0 - 3.1 g) was dissolved in distilled water (60 ml) at 80 °C for 0, 20, 40, and 60 min under continuous stirring using a magnetic stirrer. At the same time, H_3BO_3 (0.645 - 2.0 g) was dissolved in distilled water (30 - 45 ml, according to the amount H_3BO_3) (Table 1) at 60 °C for 0 - 60 min under continuous stirring by a magnetic stirrer. The H_3BO_3 solution was then slowly added to the PVA solution at 80 °C under continuous stirring for approximately 5 min. The composition ratio of PVA/H_3BO_3 and amounts of PVA and H_3BO_3 are listed in Table 2. The PVBO white gel agglomerated on the surface of the reaction mixture 5 min and 60 min after the gel was collected, or the process was continued until the water in the condensation solution evaporated. The synthesis of PVBO was completed at 80 °C under constant stirring. The white gel of PVBO or its precursor was dried at 120 °C for 24 h in an oven (Elektro-mag, M5040P) and ground by an agate mortar (Retsch Planetary Ball Mill-PM100). After the precursor powder was screened under 250 μm, it was charged in a porcelain crucible. Further, the samples were calcinated at 500, 600, and 700 °C for 1, 2, and 3 h in air by using a chamber furnace (Protherm, PLF 140/5). The samples were ground using an agate mortar and uniaxially compacted with a cold press. The sample was then placed in an alumina boat and heat treated for B_4C reduction in a tube furnace at 1400 °C under Ar flow (800 ml·min^{-1}) for 5 h at a heating rate of 8 °C·min^{-1}. After the reduction was completed, the sample was cooled to room temperature under an Ar flow 800 ml·min^{-1}). The full experimental procedure is shown in Figure 1.

Table 1. Amount of H_3BO_3 and composition ratio of H_3BO_3:H_2O.

Code	H_3BO_3 (g)	H_3BO_3 (g):H_2O (ml)
HW101	2.0	2:45
HW151	1.33	1.33:45
HW201	1.0	1:30
HW251	0.8	0.8:30
HW311	0.645	0.645:30

Table 2. Composition ratio of PVA/H_3BO_3 and amounts of PVA and H_3BO_3.

Code	PVA:H_3BO_3 ratio	PVA (g)	H_3BO_3 (g)
PHD101	1.0:1	2.0	2.0
PHD151	1.5:1	2.0	1.33
PHD201	2.0:1	2.0	1.0
PHD251	2.5:1	2.0	0.8
PHD311	3.1:1	2.0	0.645

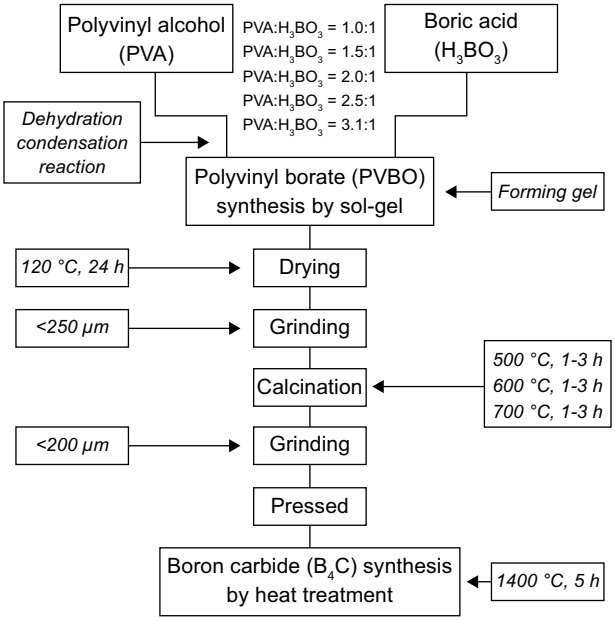

Figure 1. B_4C synthesis procedure.

Characterization

The PVA–water solution concentration (PWC_{AR}) was determined according to the formula presented below.

$$PWC_{AR} = \frac{[P_{SW} - (P_{SW} \times 5/100)]}{PDW_W - P_{RW}} \times 100,$$

where P_{SW} is the initial weight of PVA, P_{RW} is the PVA remaining after removing the weight of the volatiles in the PVA (5 %, according to technical data sheet of the product), and PW_W is the weight of the PVA–water solution after heating.

The concentration of the H_3BO_3–water solution (HWC_{AR}) was determined according to the following formula:

$$HWC_{AR} = \frac{H_{SW}}{HW_W - H_{SW}} \times 100,$$

where H_{SW} is the initial weight of H_3BO_3 and HW_W is the amount of the H_3BO_3–water solution after the preparation. In addition, H_3BO_3 was dissolved in water and the structure was protected such that the H_3BO_3 dissolved in the water would remain at similar amounts. The C/B_2O_3 mole ratio (CB_M) of the reactant after calcination was calculated using the solubility of B_2O_3 in water. First, the reactant was charged in distilled water and continuously stirred at 80 °C for 20 min. Carbon and B_2O_3 were able to separate from each other in water. The reactant–water mixture was filtrated, leaving carbon particles in the filter. The filter and carbon particles were then dried at 80 °C for 30 min. Thus, the amount of B_2O_3 was calculated by subtracting the amount of carbon from the amount of the reactant. The C/B_2O_3 mole ratio (CB_M) of the reactant was measured as follows [35]:

$$CB_M = 5.8 \times \frac{(DCF_W - F_W)}{(R_W - DCF_W - F_W)} = 5.8 \times \frac{C_W}{(R_W - C_W)},$$

where R_w is the weight of the reactant, F_W is the weight of the filter, and DCF_W is the combined weight of the carbon and filter after drying. In addition, C_W is the weight of the carbon in the reactant and could be determined through DCF_W-F_W [35].

The molecular weight of the PVA was determined using a 1260 Infinity II Gel Permeation Chromatography (GPC)/Size Exclusion Chromatography (SEC) System (Agilent Technology). The pH of each solution was measured using an Isolab, portable pH/mV meter. Each solution composition was measured five times and averaged. The viscosity of the solutions was measured using a viscometer (Brookfield Dial Reading, RVT230). The bonding structure of the PVBO was obtained using a Spectrum Two Fourier Transform Infrared (FT-IR) Spectrometer (PerkinElmer) with attenuated total reflectance (ATR) methods. The precursor powders, reactant and B_4C powder were analyzed through an XRD analysis (Bruker D2 Phaser) with CuK_α radiation. The calcined and filtered powders were observed using SEM/EDS (Phenom) at 20 kV. The microstructures of reactants and B_4C powder were evaluated using field-emission scanning electron microscopy (FESEM)/EDS (FEI Marka Quanta FEG 450).

RESULT AND DISCUSSION

Solution densification parameters

Concentration of PVA–water solution

The range of molecular weights of the PVA was measured using GPC as 19000 - 24015 g·mol^{-1}. The molecular weight of the polymeric material affects the characteristic properties, such as the viscosity, solubility, stability, water absorption capability, flexibility, and

crystallinity, during the dehydration–condensation reaction. In addition, the molecular weight is an indicator of the polymeric chain range, decreasing as the molecular weight decreases, and BO_3 molecules become unable to find opportunities to bond with carbon on the polymer backbone. Therefore, different PVA:H_3BO_3 compositions were investigated to determine the effects of PVBO formation on B_4C production (Table 2). [40].

The degree of hydrolysis is another parameter determining the properties of the polymeric material. If the degree of hydrolysis is low, the water absorption and solubility will increase; however, the viscosity will decreases in the PVA–water solution [41]. In this study, PVA with a hydrolysis degree of 87 - 89 % was used. This type of PVA provides advantages when dissolved in water owing to the low viscosity and high solubility of the PVA, which are required to increase the surface activity between the PVA and H_3BO_3 during gelation [37].

The solubility of the PVA may vary with the PVA:H_2O ratio and temperature. Fully and partially hydrolyzed PVA is soluble in water, depending on the hydrolyzation and degree of polymerization [42]. Fully hydrolyzed PVA (> 99 %) only dissolves in hot water, whereas PVA with 87 - 89 % hydrolysis is soluble in both cold and hot water. Fully hydrolyzed PVA contains strong hydrogen bonds among the hydroxyl groups in the PVA molecules after the acetate groups are removed through hydrolyzation. The hydrogen bonds lead to a decrease in the interactions among the molecules in the PVA–water solution because such bonds reduce the solubility of PVA in water. Partially hydrolyzed PVA has acetate groups between the molecules, reducing the binding effect of hydrogen. Therefore, partially hydrolyzed PVA is readily soluble in water, regardless of the temperature [43]. However, the amount of PVA dissolved in water changes depending on the temperature [44]. In a previous study, partially hydrolyzed PVA was dissolved at 80 °C for 1 h [28, 38]. The solubility rate of the PVA in water increases with an increase in the temperature during gel formation,

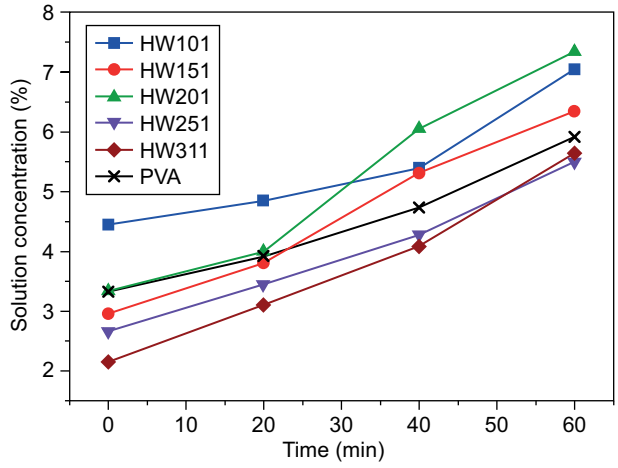

Figure 2. Solution concentration–time curves of H_3BO_3 (HW101, HW151, HW201, HW251, HW311) and PVA.

increasing the interaction between the PVA and H_3BO_3 molecules. Thus, more H_3BO_3 can be added to the PVA–water solution during gelation by increasing the temperature [44]. By contrast, the solubility ratio of the PVA in water with an increase in temperature is unstable. The stability of the PVA:H_2O ratio can be disrupted for a few reasons. First, some of the water evaporates during the heating process. Second, the rate of PVA decreases with the removal of volatiles in the PVA structure. In brief, the PVA–water solution concentration is affected by the evaporating water and volatiles. In this study, the initial PVA:H_2O ratio in the solution was determined to be 3.3 wt. %. In addition, the average concentration of the PVA was measured as 6.0 wt. % at the end of the PVA–water solution preparation.

Concentration of H_3BO_3–water solution

Boric acid (H_3BO_3) starts dehydrating at above 80 °C, and can be transformed into metaboric acid (HBO_2) [45]. The H_3BO_3–water solution was prepared at 60 °C to prevent it from becoming HBO_2 and to allow only H_3BO_3 to remain in the water. The ratio of H_3BO_3 to distilled water is in the range of 2.15 wt. % to 4.50 wt. %, depending on the PVA:H_3BO_3 ratio. The initial ratio of H_3BO_3 to distilled water increases owing to the evaporation of the water. Therefore, the initial ratios of the solution should be less than the solubility limit of H_3BO_3 in water at 60 °C owing to the evaporation of water in the solution and the dehydration of H_3BO_3. The ratio of H_3BO_3 to water is between 4.5 wt. % and 7.5 wt. % after the dissolving process. In a previous study, the solubility limit of H_3BO_3 in water was shown to be 4.72 wt. % at 20 °C, 15.75 wt. % at 70 °C, and 19.10 wt. % at 80 °C. If H_3BO_3 is added to the water at a higher amount than its solubility limit, it cannot dissolve completely during the heating process [15, 46]. In addition, an excess H_3BO_3 concentration prevents a uniform composition dispersion [27]. The highest solution concentration is obtained from the HW201 sample in Figure 2. It can be deduced that the solubility and distribution of H_3BO_3 in water is greater than those in the other solutions, and that H_3BO_3 can bond to the PVA structure more effectively.

Temperature, viscosity, and pH of PVA–water solution

Increasing the temperature directly affects the viscosity and solubility of the PVA solution. The aim of heating during the solution step is to increase the solubility, decrease the viscosity, and hinder the agglomeration. Partially hydrolyzed PVA can be dispersed in water at room temperature and partially dissolved, but not completely. Heating is necessary to dissolve PVA. In the literature, fully hydrolyzed PVA was dissolved at 80 °C for 1 h [38]. However, the temperature was insufficient to dissolve the PVA. Added water to increase the solubility of the PVA, This further decreased the viscosity [38].

As shown in Figure 3, a viscosity of 7.3 cP and a pH value of 6.25 were measured for a constant PVA–water solution at 80 °C. The pH value and viscosity of the sol decrease as the temperature increases. Partially hydrolyzed PVA can be dissolved easily in hot distilled water with continuous stirring, and the fluidity is increased. As the viscosity decreases, the mobility and stability of the sol increase at a constant temperature [39]. Thus, the dispersion of particles in the PVA–water solution increases during gelation. Further, lowering the solution viscosity can reduce the amount of B_2O_3 and increase its dispersion in the polymeric precursor [37, 38]. In addition, if the PVA-water solution becomes more acidic, the viscosity of the solution decreases and the particle dispersion increases [39]. As a result, 80 °C was chosen for dissolving the PVA in water and providing the highest dispersion of H_3BO_3 in PVA-water solution.

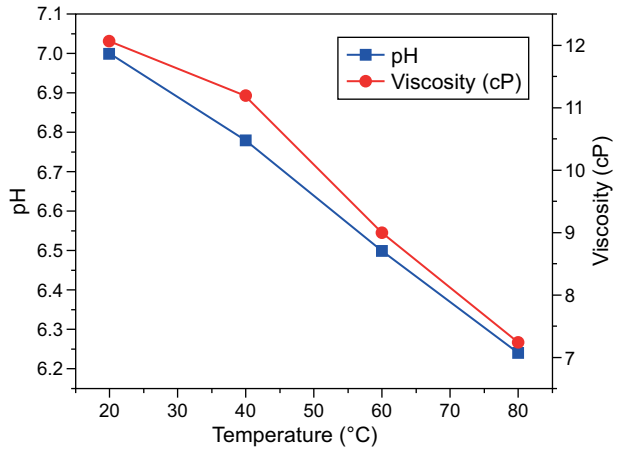

Figure 3. Relationship among temperature, viscosity, and pH value of PVA–water solution (PVA:H_2O ratio fixed at all compositions).

Temperature dependence of the pH of H_3BO_3–water solution

The H_3BO_3–water solution is weakly acidic. This property can arise from the following factors. Temperature decreases the pH values of the PVA–water and H_3BO_3–water solutions. Because the water ionizes, the amount of H ions increases in the solution and the pH value decreases. In addition, H_3BO_3 dissolves in water, and its solubility ratio increases with an increase in temperature. During the dissolution of H_3BO_3, H_2O molecules and positive ions such as H_3O^+ are lost. H_3O^+ ions can decrease the pH value of the H_3BO_3–water solution [47]. The boron alkoxides are hydrolyzed to Reaction 1 and B-OH react with H^+ ions Reaction 2 [39]. Thus, the pH value of H_3BO_3–water can decrease at higher temperatures, and H_3BO_3 can bond with PVA more effectively.

$$B–OR + H_2O \rightarrow B–OH + ROH \quad (1)$$

$$B–OH + H^+ \rightarrow B–OH_2^+ \quad (2)$$

The pH value and solution concentration were measured for all samples at 20, 40, 60 °C. The pH-temperature relationship for all samples during 60 min process is given in Figure 4. It is observed that the pH value decreases by increasing the solution temperature, regardless of the composition ratio. However, the amount of H_3BO_3 in water affects the pH value in a decisive way (Higher H_3BO_3 leads to decrease the pH value). Thus, the lowest pH value and highest solution concentration were obtained from HW101 at different temperatures (Figure 4). The results suggest that H_3BO_3 can be more efficiently soluble in water for HW101 sample than the other.

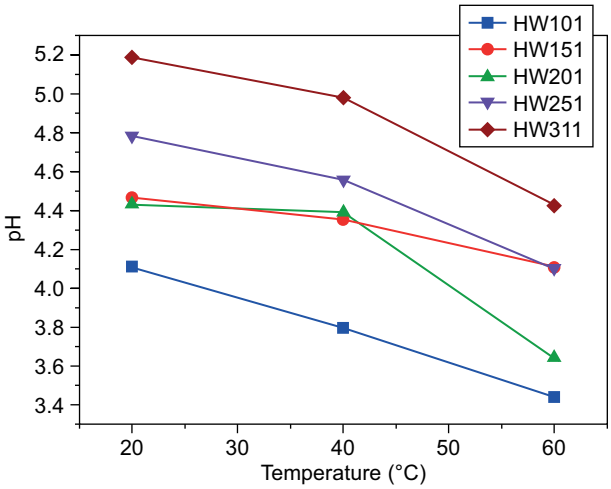

Figure 4. Temperature dependence of the pH value for all samples during 60 min process time.

Parameters of PVBO gelation synthesis

Effect of temperature on condensation of PVBO

During the gelation process, the H_3BO_3 solutions were slowly added to the PVA solutions. The temperature was fixed at 80 °C to facilitate the dehydration–condensation reactions. The H_3BO_3 reacted with the PVA immediately when it was added because the –OH ions in the H_3BO_3 easily bond with the hydroxyl groups in the PVA. The hydrogen bonds provided a cross-linking structure in the PVA chain [48] such that the viscosity increased in the PVA–water solution and produced a gel. When the H_3BO_3 solutions were rapidly charged in the PVA solutions, the agglomeration was carried out on the surface of the PVA solution, and B–O atoms were unable to react at the interface of the PVA–H_3BO_3.

Effect of pH on condensation of PVBO

The relationship between the pH value and the ratio of PVA/H_3BO_3 (see the sample codes in Table 2) the PVA, H_3BO_3, and gel is shown in Figure 5. When

the concentration of H_3BO_3 in the H_3BO_3-water solution increased, the pH value of the H_3BO_3–water solution decreased due to the increasing acidity of the solution. The ratio of H_3BO_3 was higher than in the initial H_3BO_3:H_2O ratio due to the evaporation of water. The amount of water affects the ratio of concentration and the pH value. In this study, the water volume of HW311, HW251, HW201 was 30 ml, whereas 45 ml of water was used for HW151 and HW101. When the same amount of water (30 ml) was used in all samples, the H_3BO_3 was thoroughly dissolved at the start. Later, some of the water in the solution evaporated by heating, and H_3BO_3 precipitated owing to the insufficient amount of remaining water, which exceeded the solubility limit of H_3BO_3. Therefore, 45 ml of water was used for PHD151 and PHD101.

Ester and complex bonds formed during the reaction between PVA and H_3BO_3 via the dehydration–condensation mechanism. In addition, H_3BO_3 was unable to react completely with PVA and remained in the water solution. The higher H_3BO_3 ratio provided an increased possibility of a reaction between PVA and H_3BO_3. Further, H_3BO_3 was dissolved in water through hydrolysis. Thus, protons were released, and the pH value of the solution gradually decreased during gelation, see [49]. This situation indicates that the agglomeration decreased. In this study, the pH value of the PVA solution at 80 °C is approximately 6.25. This value could lead to an agglomeration of the PVA when in contact with H_3BO_3. The pH range of the H_3BO_3 was 3.5 - 4.5. This ratio provided a more acidic condition during the gelation step, and the agglomeration decreased [39]. However, it was insufficient to prevent the agglomeration during the gel formation. The pH range of the gel solutions, as shown in Figure 5, was 4.9 - 5.7. In addition, if the pH value of PVA-water solution becomes more acidic, the particle dispersion increases [39]. In previous studies, the pH of gel solution was kept below 5.0 [30, 35, 39]. The pH value of PHD101 was under 5.0 and the pH value of other sample was above 5.0. Therefore, the agglomeration of PHD101 took longer than that of the other samples and increased the dispersion of H_3BO_3 in the PVA solution and the formation rate of the PVBO.

Effect of time on condensation of PVBO

In previous studies, the condensation process was completed with a thorough evaporation of water [27, 30, 36, 38]. The gelation occurred within 5 min, and PVBO was obtained as a white gel. The stirring and heating processes were continued until the water was completely evaporated. During PVBO formation, the hydroxyl groups, which separated from H_3BO_3, bonded to the C atoms in the PVA chain. However, not all H_3BO_3 dissolved in water was able to react with the PVA gel within 5 min, and some of the dissolved H_3BO_3 remained in the aqueous solution. In other words, not all boron atoms were able to contact the C atoms initially. Thus, the product of the condensation process was analyzed at different holding times.

First, we determined three different conditions according to the time and water evaporation conditions. The first and second conditions were based on the completion of the process at 5 and 60 min, respectively. The third condition was based on the complete evaporation of the water after gel formation. The gel structure varied with the condensation time. When the gel was taken from the beaker at 5 or 60 min, the gel structure became sponge like. When the water was allowed to evaporate completely, the structure of the gel became rubbery and was coated with a H_3BO_3 powder. In addition, the weights of the gels formed were measured after 5 min of condensation and after the completion of the evaporation. It was shown that the gel weight is greater after the short-term condensation process in Figure 6. The longer condensation process promoted a lighter gel weight. PVA underwent high water absorption and the solution absorbed the water during the condensation reaction. The gel was constantly exposed to stirring and

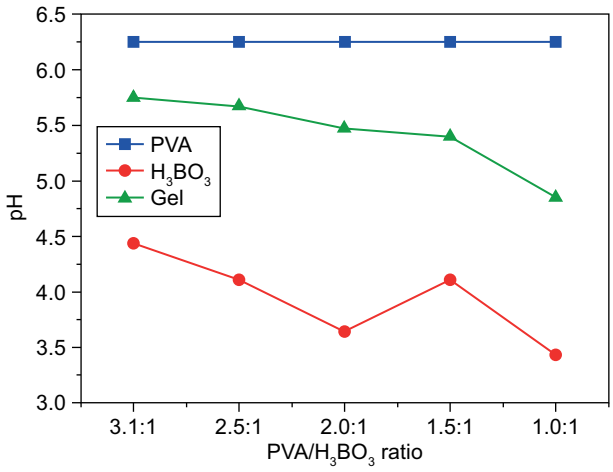

Figure 5. Dependence of the pH on the PVA/H_3BO_3 ratio for PVA, H_3BO_3, and gel.

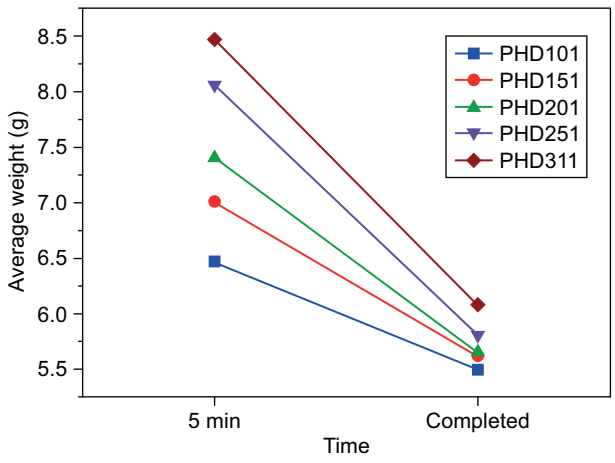

Figure 6. Relationship between average gel weight and PVBO formation time in PHD samples.

an applied temperature during a longer processing time. During this time, the gel formed left the absorption water and became more rigid. All samples contain the same amount of PVA. For this reason, the water absorption behavior can be expected to be similar for each sample, and the average gel weight is expected to be very close. However, the average gel weight is different for all samples presumably because of the different amount of H_3BO_3.The variation of samples weight can be attributed to the effect of H_3BO_3. PHD101 contain the highest amount of H_3BO_3, and the lightest amount of gel weight was obtained from it, regardless of gelation time. In addition, as the H_3BO_3 ratio decreases in the samples, the gelation weight increases. For these reason, it can be deduced that higher amount of H_3BO_3 can be bonded with PVA much more easily and prevent the water absorption of PVA.

When the gelation process was finished and the gel was removed, aqueous solution remained under the first and second conditions, whereas a sediment was observed under the third condition. The remaining aqueous solutions were fully dehydrated at 120 °C, and the deflocculated products also settled in the form of sediments. All sediments were weighed. The difference in weight between the sediment samples with respect to time is shown in Figure 7. Most of the sediment measured was in PHD101, which included the highest amount of H_3BO_3 among the samples. All samples contained the same amount of PVA and the same PVA "structural capacity" in terms of bonding to H_3BO_3. This capacity is maximized in the PHD101 sample, in which a higher amount of H_3BO_3 appears as a sediment than in the other samples. Therefore, excessive H_3BO_3 could not bond to the PVA and remained in the PVA–H_3BO_3 gel solution. The average amount of sediment also decreased as the amount of H_3BO_3 gradually decreased. The ratio of the condensation reaction could increase between the H_3BO_3 and PVA molecules with respect to temperature and time. In addition, the partially hydrolyzed PVA absorbed much more water during dissolution. It could lose water from the structure and increase contact with more of the H_3BO_3 molecules. Thus, the amount of sediment should decrease over time.

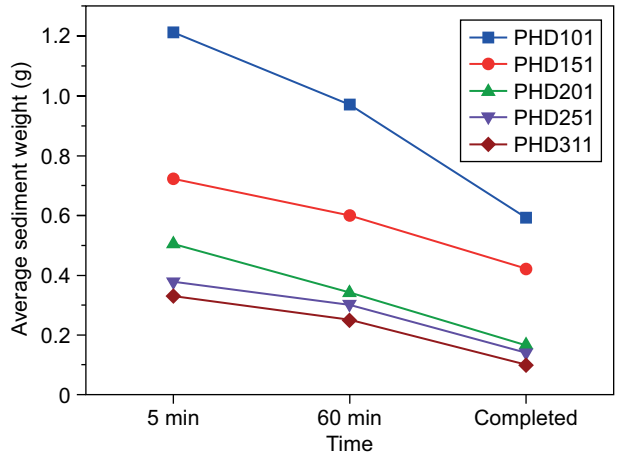

Figure 7. Relationship between sediment weight and time of the PVBO synthesis process in PHD samples.

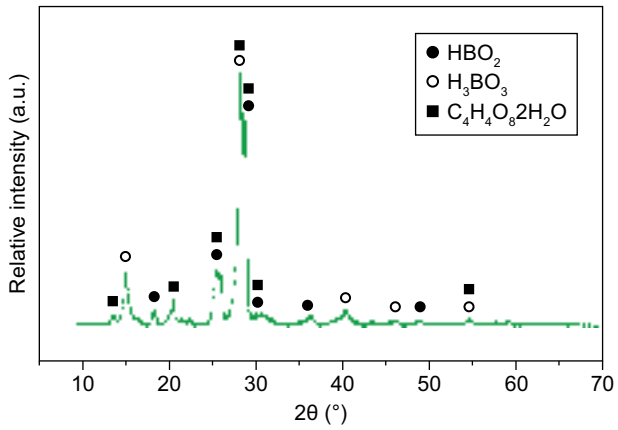

Figure 8. XRD pattern (diffractogram) of the sediment after drying at 120 °C for PHD101.

The XRD pattern of the sediment for PHD101 is shown in Figure 8. The sediment contained HBO_2, H_3BO_3, and $C_4H_4O_6{\cdot}2H_2O$ phases. The intensities of the peaks of all crystalline phases in the XRD were high. In addition, H_3BO_3 in the XRD diffractogram came from initial H_3BO_3, and did not react with the partially hydrolyzed PVA. When the H_3BO_3 powder did not react with the PVA, it remained in the sediment, which consisted of a mixture of H_3BO_3 and PVA powder. The H_3BO_3 was dehydrated at 120 °C during the drying process. Therefore, it transformed into an HBO_2 phase. The partially hydrolyzed PVA consisted of $C_4H_6O_2$ and C_2H_4O. Phase peaks of $C_4H_4O_6{\cdot}2H_2O$ in the XRD pattern formed as a result of the reaction between PVA and H_2O. The XRD spectra of the sediment primarily included crystalline phases. Thus, it was deduced that the ratio of PVA could be lower than the ratios of H_3BO_3 and any other borate phases in the sediment, and a large amount of PVA was passed to the gel structure.

Investigation of PVBO

XRD analysis

PVA is a semicrystalline material. H_3BO_3 bonds to the amorphous region of the PVA and H_3BO_3 increases the chain length of the amorphous structure [50]. XRD analyses of the PVA and PVBO are shown in Figure 9. The characteristic peak of the PVA is observed at 2θ = = 19.5°. This peak also appears in the PVBO samples, but in a much more broadened form, which shows that an esterification reaction occurs between the H_3BO_3 and PVA. As to the 2θ = 40° peak, it disappears in the PVBO samples. All sample peak intensities and widths are extremely similar, and thus it is difficult to assess the formation rate of the PVBO with respect to the initial composition ratio. Mondal ve Banthia et al. [22] analyzed the polymeric precursor structure using

XRD, and observed some crystalline peaks in the diffraction pattern. In this study, only one peak (2θ = 28°) was observed in the XRD analysis for PHD201, and all PVBO samples showed generally amorphous characteristics. A large hump (2θ = 19.5°) was observed only in the XRD pattern of the PVBO [29]. Barros et al. [29] reported such a diffraction pattern attributing it to the semi-crystalline structure of the polymeric precursor. As a result, similar XRD patterns were observed in this study for the PVBO samples. Therefore, according to the XRD analysis, it can be deduced that the synthesis of PVBO was successful.

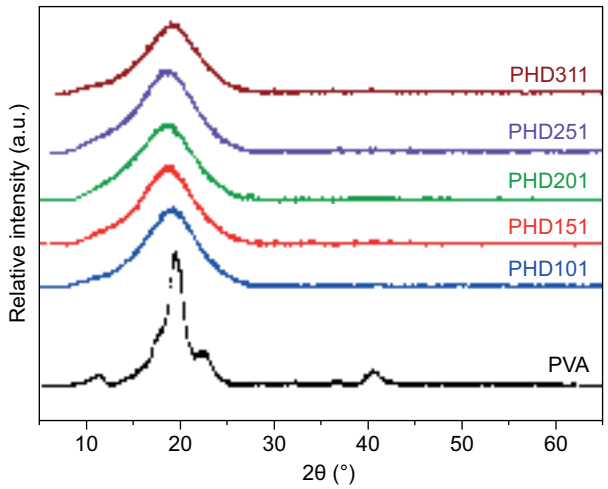

Figure 9. XRD analyses of PVBO.

FTIR analysis

According to the XRD analyses, PVBO was synthesized from all PHD samples. The sample containing the highest proportion of H_3BO_3, i.e., HW101, had the highest solution concentration, and its pH was lower than that of the other samples. This led to a decrease in the pH of PVA–H_3BO_3, which was the solution with the lowest-pH, during the gelation. The solution became more acidic and the degree of agglomeration decreased compared to the other samples. Therefore, the dispersion of H_3BO_3 in the PVA was higher than in the other solutions. In addition, as the amounts of H_3BO_3 increase in a sample, it can be bonded with PVA further and prevent the water absorption of PVA (Figure 6). As a result, the study continued based on the PHD101 sample, which was investigated using FTIR to prove the formation of PVBO.

The FTIR spectra of H_3BO_3, PVA, and PHD101 are shown in Figure 10. The O–H stretching vibrations appeared at absorption bands of 3000 - 3500 cm^{-1} for H_3BO_3, PVA, and PVBO. If the O–H bond peaks are lower at the PVBO spectrum, this indicates that esterification reactions occur between the PVA and H_3BO_3. However, there are unreacted O–H bonds in the PVBO [27, 34]. The absorption peak at 1450 cm^{-1} is attributed to the B–O bonds [22]. These peaks can be seen in both the PVBO and H_3BO_3 but are smaller in the PVBO. In addition, C–O–C bonds are observed in the absorption bands at ~1250 cm^{-1} in the PVA spectra, but are absent in the PVBO. The B–O–H bonds appear at ~1190 cm^{-1} in the H_3BO_3 spectra and can be seen in the PVBO spectra, because B–O–H bonds are maintained in the PVBO [35]. Some H_3BO_3 molecules could not react with the PVA and remained in the PVBO structure. Moreover, the peak at 2952 cm^{-1} is referred to the aliphatic vibration of the C–H bonds, which are not found in the PVBO spectra [22]. The 1287 cm^{-1} and 1080 cm^{-1} absorption peaks were ascribed to the B–O–C bonds, which are the main evidence for the formation of PVBO [26, 27, 31, 34]. Therefore, condensation reactions were executed between the PVA and H_3BO_3. The C–H peaks were not seen in PHD101, which contained the highest amount of H_3BO_3 among all samples. C–H peaks were present in the PVA. The C–O–C and B–O–H bands disappeared in the PVBO sample. The intensity of the peaks gradually decreased because of the decreasing H_3BO_3 content. The C–O from the PVA and B–O–H from the H_3BO_3 bands intensity decreased in the PHD101. As a result, PHD101 is preferred for further analysis because H_3BO_3 is bonded with the PVA structure and the formation of PVBO is maximized.

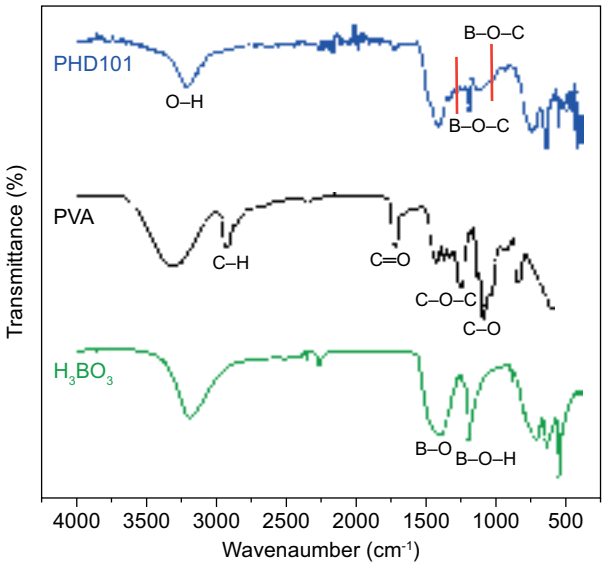

Figure 10. Comparison of FTIR spectra of H_3BO_3, PVA and PHD101.

Calcination

The polymeric precursor was calcined to decompose the organic compounds. Borate ester bonds in the polymeric precursor were destroyed through heat treatment and yielded a reactant composed of finely distributed B_2O_3 in a C matrix. Thus, the single-source reactant served as a carbon and boron source for B_4C

synthesis. SEM images of the PHD101 reactant and B_2O_3 leaching from the reactant are shown in Figure 11a and b, respectively. Five points are shown on the SEM images and their EDS analysis results are listed in Table 3. At points 1 and 4, both B and O were detected, indicating the presence of B_2O_3. At points 2 and 3, B, O, and C were observed, which indicates that the product consisted of B_2O_3 and carbon. At point 5, B_2O_3 molecules were dissolved by hot water and left the carbon matrix, and thus a significant number of carbon atoms can be seen in the EDS analysis results.

The molar ratio of C/B_2O_3 stoichiometric B_4C synthesis should be 3.5, according to reaction 3.

$$2B_2O_3 + 7C \rightarrow B_4C + CO \quad (3)$$

However, B_2O_3 transforms into boron suboxides with heat. The boron suboxides are in a vapor phase at above 1050 °C and leave a reaction zone [22, 27]. Therefore, the molar ratio of C/B_2O_3 should be less than 3.5 to compensate for the volatile boron suboxide. Yanase et al. [27] reported that calcination should be performed at 600 °C in air for 2 h to optimize the C/B_2O_3 molar ratio, which was measured as approximately 3.3. In previous studies, it was suggested that C/B_2O_3 should be approximately 2.9 - 3.5 [28, 37]. The composition of the initial raw materials should be adjusted to the molar ratio of C/B_2O_3.

The calcination step was applied at 500, 600, and 700 °C in air for 1 - 3 h. Calcination was conducted at above 400 °C in order to decompose of the polymeric precursor and remaining polymeric groups [37]. The process was executed in air according to [51]. The free carbon content in B_4C could be reduced via carbothermal reduction of the reactants below 1800 °C, leading to a homogeneous and uniform reactant component distribution [38]. The range of the C/B_2O_3 ratios was calculated for the PHD101 sample, as listed in Table 4. H_3BO_3 either enters the gel structure molecularly via a condensation reaction with the PVA or adheres to the gel as a particle and remains in the gel structure. As a result, the C/B_2O_3 ratio is unstable. The C/B_2O_3 ratio of samples were measured and calculated according to the condensation process (5 min and complete water evaporation). We determined the range of C/B_2O_3 for each calcination temperature and time. We observed that the amounts of carbon and B_2O_3 vary with the gelation time, obviously because the condensation reactions between PVA and H_3BO_3 continue during the gelation. When excessive

Table 3. EDS analysis results of PHD101.

EDS points	Element symbol	Atomic conc. (%)	Weight conc. (%)
1	O	70.38	77.86
	B	29.62	22.14
2	C	59.51	54.32
	O	31.47	38.27
	B	9.01	7.40
3	C	61.40	55.68
	O	32.72	39.52
	B	5.88	4.80
4	O	75.14	81.73
	B	24.86	18.27
5	C	69.13	62.26
	O	30.48	36.57
	Ca	0.39	1.17

Table 4. C/B_2O_3 ratio in the reactant from PHD101.

Time (h)	Temperature (°C)		
	500	600	700
1	3.98 - 1.96	2.93 - 1.20	2.24 - 0.66
2	3.34 - 1.80	2.50 - 0.96	1.79 - 0.57
3	3.01 - 1.64	2.32 - 0.80	1.71 - 0.46

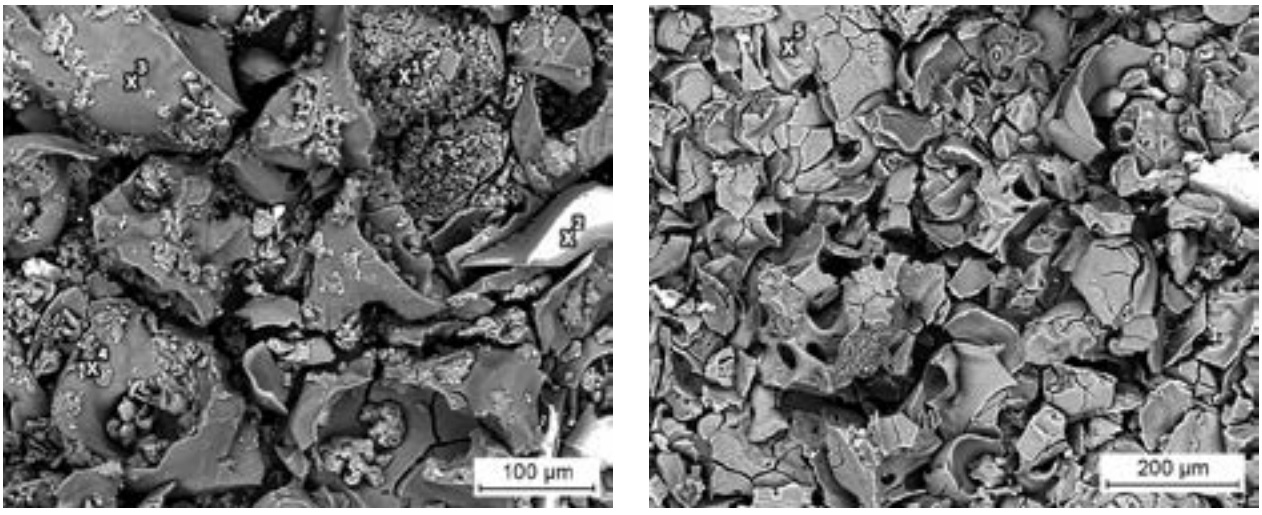

a) b)

Figure 11. SEM images of: a) PHD101 reactant calcined at 500 °C for 2 h and b) B_2O_3 dissolved for the same sample.

H_3BO_3 is present in the solution, the PVA cannot react with all dissolved H_3BO_3. The remaining H_3BO_3 powder is deposited on the gel surface formed. Therefore, the ratios of C/B_2O_3 change with gelation time. Based on literature data [28, 37], a calcination temperature of 500 °C with a dwell time of 2 h was chosen for achieving an optimum ratio of C/B_2O_3 for in the PHD101 sample.

The FESEM image of the PHD101 sample after extraction of B_2O_3 from the reactant is given in Figure 12. The PVA has a reticulated structure that affects the distribution of H_3BO_3 molecules [28]. After calcination, the structure is responsible for the distribution of B_2O_3 in the carbon structure. The reactant was washed in hot water. The B_2O_3 then dissolved and left the carbon matrix. A porous structure could be seen in the carbon matrix. The estimated pore size distribution of FESEM image obtained from the reactant is given Figure 13. The pore size distribution was non-uniform, with an average pore size was of approximately 150 nm. B_2O_3 was distributed nearly homogeneously on the nano-scale level in the carbon matrix (Figure 12). Some larger pores can be seen in the image because unreacted H_3BO_3 powder with the PVA–water solution precipitated and remained in the PVBO gel. The H_3BO_3 powder was calcined and transformed into B_2O_3. These pores formed by dissolution of B_2O_3 in water at 80 °C.

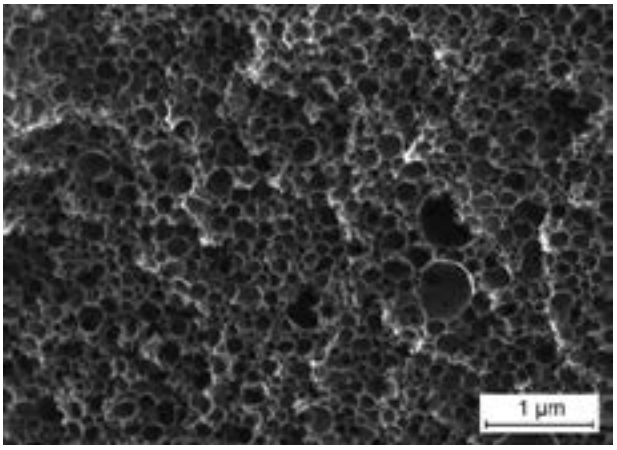

Figure 12. FESEM image of PHD101 sample after calcination at 500 °C for 2 h (after B_2O_3 was extracted from the C/B_2O_3 reactant).

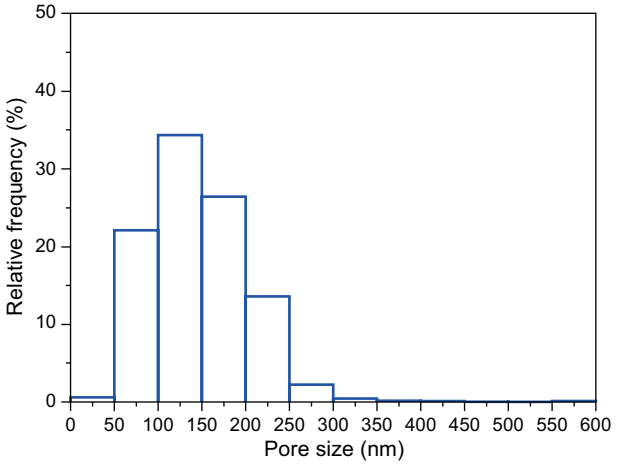

Figure 13. Pore size distribution of PHD101 sample at 500 °C for 2 h calcination after B_2O_3 was extracted from the C/B_2O_3 reactant estimated from FESEM image.

B_4C synthesis

The XRD pattern of PHD101 after calcination at 500 °C for 2 h is given in Figure 14a. The peaks of B_2O_3 and C are clearly seen on the XRD pattern. These peaks provide correlation with SEM analysis of reactant in Table 3. In addition, H_3BO_3 phase is found the reactant structure. Probably, this H_3BO_3 phase results from B_2O_3 being in contact with moisture in the air. After heat treatment at 1400 °C for 5 h the B_2O_3 has disappeared and amount of carbon is has decreased (Figure 14), indicating that B_2O_3 has reacted with carbon according to reaction (3) to form B_4C. An XRD pattern is shown in Figure 14b, where the crystalline peaks of B_4C are clearly observed. Silicon Carbide (SiC) has formed as an impurity. Also the free carbon can be considered as an impurity. The B_2O_3, which is in the reactant, can be transformed into vapor phase suboxides and might leave the reactant structure. Therefore, the carbon is unable to find enough B_2O_3 to react quantitatively and remains as free carbon in the B_4C material. The B_4C crystalline size was determined by the Scherrer equation. The calculated average crystallite size was 24 nm.

The SEM/EDS analysis is shown in Figure 15. Si was observed in the EDS analysis, and the XRD and EDS

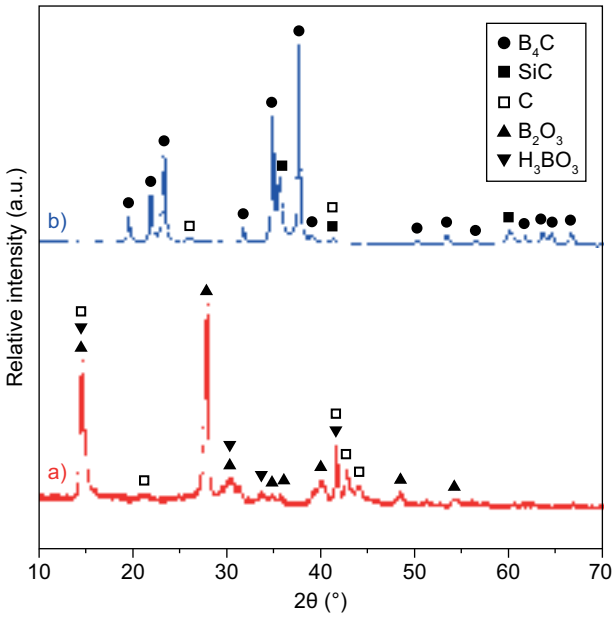

Figure 14. XRD analysis of PHD101 sample after heat treatment at 1400 °C for 5 h (a), before calcination at 500 °C for 2 h (b).

analyses provide a correlation of the presence of Si in the product, which must be considered as a result of contamination. Moreover, aluminum was found in the EDS analysis (however, no aluminum-containing was detected by XRD analysis.) This is probably a contamination coming from the alumina crucible. The B_4C structure can clearly be seen in the SEM analysis, and the EDS peaks confirm this composition. However, some parts of the structure is covered with whitish particles, which were analyzed using EDS and identified as having a Si peak higher than the B peak. SiC accumulated over the B_4C structure and entered the structure during the reduction reactions.

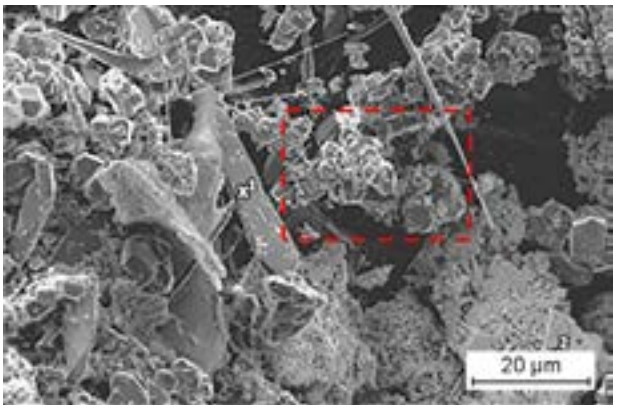

a)

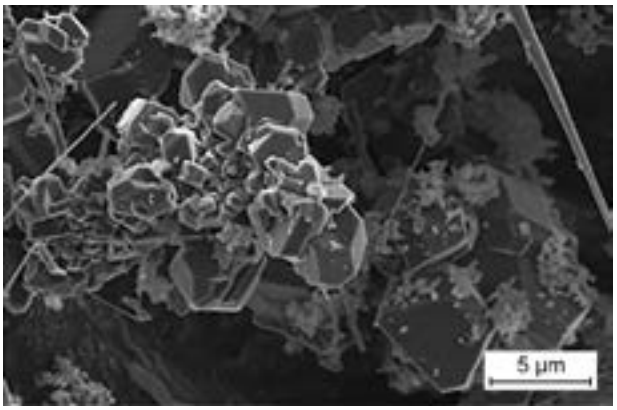

b)

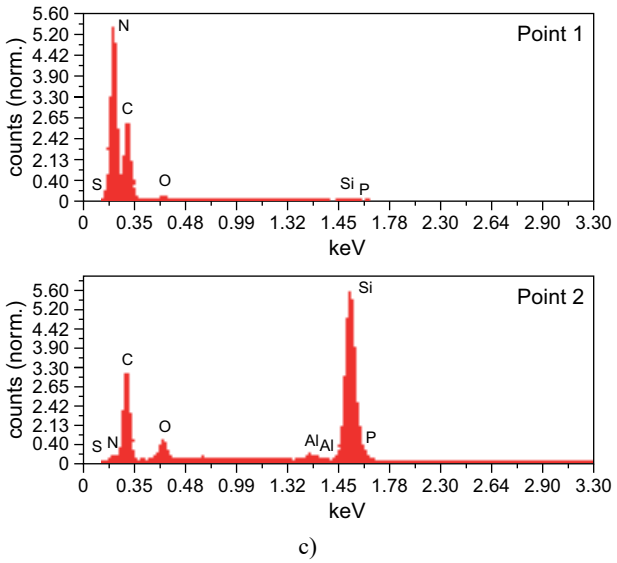

c)

Figure 15. a) SEM micrograph, b) magnified area which marked with red rectangle dashed lines in (a), and c) EDS analysis of PHD101 sample after heat treatment at 1400 °C for 5 h (before calcination at 500 °C for 2 h.)

Polygonal grains were found in the morphology of the sample (Figure 15a, b). These grains forms aggregated particles, comprising both fine and irregular shapes. The particle size distribution was extremely wide. In addition, polyhedral, needle-like, and flake-like particles were observed. Different morphological shapes can be the results of different nucleation mechanism. Polyhedral B_4C is expected to arise from the synthesis reaction between liquid B_2O_3 and solid carbon [52], whereas needle-like and flake-like B_4C particles are expected to form via vapor and solid mechanisms between the B_2O_3 and carbon molecules. As a result, a morphologically non-uniform B_4C material was synthesized by heat treatment at 1400 °C for 5 h.

CONCLUSION

In this study, industrial raw materials, including partially hydrolyzed PVA and technical-grade H_3BO_3, were used for B_4C synthesis using a polymeric precursor method distinct from that applied in existing studies (in terms of raw materials). PVBO was produced through a sol-gel method. The condensation process parameters were investigated, including the pH value and viscosity, and the temperature was determined based on the composition ratio during the solution preparation process. A viscosity of 7.3 cP and a pH of 6.25 were measured for a constant PVA–water solution at 80 °C. The solubility of H_3BO_3 for different compositions increased when the temperature was increased. The sample containing the highest proportion of H_3BO_3, i.e., HW101, had the highest solution concentration and a lower pH than the other samples. This led to a decrease in the pH of PVA–H_3BO_3, which was the solution with the lowest pH value (4.85), during gelation. The solution became more acidic and the degree of agglomeration decreased with respect to the other samples. Therefore, the ratio of H_3BO_3 increased, and the synthesis efficiency of PVBO is better than in the other samples. According to FTIR analysis, the 1287 cm^{-1} and 1080 cm^{-1} absorption peaks are ascribed to the B–O–C bonds, which are the main evidence for the PVBO formation. Peaks of B–O–C were obtained from the PHD101 sample, which was calcined under different conditions. The polymeric precursor was calcined to decompose the organic compounds. Borate ester bonds in the polymeric precursor were destroyed by heat treatment and yielded a reactant composed of the distributed B_2O_3 in the C matrix. The optimum value

of C/B_2O_3, 3.34, was achieved at 500 °C for 2 h, with B_2O_3 being distributed at the nano-scale level in the carbon matrix. Finally, these samples were heat treated at 1400 °C for 5 h. As a result, crystalline, irregular, and polyhedral B_4C powder was synthesized from industrial-grade raw materials.

REFERENCES

1. Domnich V., Reynaud S., Haber R.A., Chhowalla M. (2011): Boron carbide: structure, properties, and stability under stress. *Journal of the American Ceramic Society*, *94*, 3605–3628. doi: 10.1111/j.1551-2916.2011.04865.x
2. Thevenot F. (1990): Boron carbide a comprehensive review. *Journal of the European Ceramic Society*, *6*, 205-225. doi: 10.1016/0955-2219(90)90048-K
3. Cicek B., Karaahmet O. (2018). *Bor karbür ve düşük sıcaklık bor karbür sentezleme yöntemleri.* 1st ed. Nobel Akademik Yayıncılık.
4. Suri A.K., Subramanian C., Sonber J.K., Murthy T.S.R.Ch, (2010): Synthesis and consolidation of boron carbide: a review. *International Materials Reviews*, *1*, 4-40. doi: 10.1179/095066009X12506721665211
5. Telle R., Sigl L.S., Takagi K. (2000). Boride-based hard materials, in: Riedel R. (Ed): *Handbook of Ceramic Hard Materials*. 1st ed, pp.802-945. Wiley.
6. Werheit H. (2016): Boron carbide: consistency of components, lattice parameters, fine structure and chemical composition makes the complex structure reasonable. *Solid State Sciences*, *60*, 45-54. doi: 10.1016/j.solidstatesciences.2016.08.006
7. Ulrich S., Ehrhardt H., Schwan J., Samlenski R., Brenn R. (1998): Subplantation effect in magnetron sputtered superhard boron carbide thin films. *Diamond and Related Materials*, *7*, 835-838. doi: 10.1016/S0925-9635(97)00306-3
8. Gogotsi G.A., Groushevsky Ya.L., Dashevskaya O.B., Gogotsi Yu.G., Lavrenko V.A. (1986): Complex ınvestigation of hot-pressed boron carbide. *Journal of the Less Common Metals*, *117*, 225-230. doi: 10.1016/0022-5088(86) 90037-8
9. Hou X., Chou K.-C. (2013): Quantitative ınvestigation of oxidation behavior of boron carbide powder in air. *Journal of Alloys and Compounds*, *573*, 182–186. doi: 10.1016/j.jallcom.2013.04.012
10. Lee H., Speyer R.F. (2002): Hardness and fracture toughness of pressureless-sintered boron carbide (B_4C). *Journal of the American Ceramic Society*, *85*, 1291-1293. doi: 10.1111/j.1151-2916.2002.tb00260.x
11. Zhang Z., Du X., Wang J., Wang W., Wang Y., Fu Z. (2014): Synthesis and structural evolution of B_4C–SiC nanocomposite powders by mechanochemical processing and subsequent heat treatment. *Powder Technology*, *254*, 131–136. doi: 10.1016/j.powtec.2013.12.055
12. Kalandadze G.I., Shalamberidze S.O., Peikrishvili A.B. (2000): Sintering of boron and boron carbide. *Journal of Solid State Chemistry*, *154*, 194-198. doi: 10.1006/jssc.2000.8835
13. Moshtaghioun B.M., Cumbrera-Hernández F.L., Gómez-García D., Bernardi-Martín S.de, Domínguez-Rodríguez A., Monshi A., Abbasi M.H. (2013): Effect of spark plasma sintering parameters on microstructure and room-temperature hardness and toughness of fine-grained boron carbide(B_4C). *Journal of the European Ceramic Society*, *33*, 361-369. doi: 10.1016/j.jeurceramsoc.2012.08.028
14. Angers R., Beauvy M. (1983): Hot-pressing of boron carbide. *Ceramics International*, *10*, 49-55. doi: 10.1016/0272-8842(84)90025-7
15. Alizadeh A., Taheri-Nassaj E., Ehsani N. (2004): Synthesis of boron carbide powder by a carbothermic reduction method. *Journal of the European Ceramic Society*, *24*, 3227–3234. doi: 10.1016/j.jeurceramsoc.2003.11.012
16. Mohantya R.M., Balasubramanian K., Seshadri S.K. (2007): Multiphase formation of boron carbide in B_2O_3–Mg–C based micropyretic process. *Journal of Alloys and Compounds*, *441*, 85–93. doi: 10.1016/j.jallcom.2006.09.069
17. Deng F., Xie H.-Y., Wang L. (2006): Synthesis of submicron B_4C by mechanochemical method. *Materials Letters*, *60*, 1771–1773. doi: 10.1016/j.matlet.2005.12.016
18. Jansson U., Carlsson J.-O., Stridh B., Söderberg S., Olsson M. (1989): Chemical vapour deposition of boron carbides I: phase and chemical composition, *Thin Solid Films*, *172*, 81-93. doi: 10.1016/0040-6090(89)90120-X
19. Ramos A.S., Taguchi S.P., Ramos E.C.T., Arantes V.L., Ribeiro S. (2006): High-energy ball milling of powder B–C mixtures. *Materials Science and Engineering A*, *422*, 184–188. doi: 10.1016/j.msea.2006.01.096
20. Heian E.M., Khalsa S.K., Lee J.W., Munir Z.A. (2004): Synthesis of dense, high-defect-concentration B_4C through mechanical activation and field-assisted combustion. *Journal of the American Ceramic Society*, *87*, 779-783. doi: 10.1111/j.1551-2916.2004.00779.x
21. Shi L., Gu Y., Chen L., Qian Y., Yang Z., Ma J. (2003): A low temperature synthesis of crystalline B_4C ultrafine powders. *Solid State Communications*, *128*, 5-7. doi: 10.1016/S0038-1098(03)00627-6
22. Mondal S., Banthia A.K. (2005): Low-temperature synthetic route for boron carbide. *Journal of the European Ceramic Society*, *25*, 287-291. doi: 10.1016/j.jeurceramsoc.2004.08.011
23. Watts J.L., Talbot P.C., Alarco J.A., Mackinnon I.D.R. (2017): Morphology control in high yield boron carbide. *Ceramics International*, *43*, 2650–2657. doi: 10.1016/j.ceramint.2016.11.076
24. Weimer A.W., Moore W.G., Roach R.P., Hitt J.E., Dixit R.S., Pratsinis S.E. (1992): Kinetics of carbothermal reduction synthesis of boron carbide. *Journal of the American Ceramic Society*, *75*, 2509–2514. doi: 10.1111/j.1151-2916.1992.tb05604.x
25. Foroughi P., Cheng Z. (2016): Understanding the morphological variation in the formation of B_4C via carbothermal reduction reaction. *Ceramics International*, *42*, 15189–15198. doi: 10.1016/j.ceramint.2016.06.126
26. Rafi-ud-din, Zahid G.H., Asghar Z., Maqbool M., Ahmad E., Azhar T., Subhani T., Shahzad M. (2014): Ethylene glycol assisted low-temperature synthesis of boron carbide powder from borate citrate precursors. *Journal of Asian Ceramic Societies*, *2*, 268-274. doi: 10.1016/j.jascer.2014.05.011
27. Yanase I., Ogawara R., Kobayashi H. (2009): Synthesis of boron carbide powder from polyvinyl borate precursor. *Materials Letters*, *63*, 91-93. doi: 10.1016/j.matlet.2008.09.012
28. Kakiage M., Tahara N., Watanabe R., Yanase I., Kobayashi H. (2013): Microstructure in precursor formed by controlling composition of condensed boric acid-poly(vinyl

alcohol) product for low-temperature synthesis of boron carbide powder. *Journal of the Ceramic Society of Japan*, *121*, 40-44. doi: 10.2109/jcersj2.121.40
29. Barros P.M., Yoshida I.V.P., Schiavon M.A. (2006): Boron-containing poly(vinyl alcohol) as a ceramic precursor. *Journal of Non-Crystalline Solids*, *352*, 3444-3450. doi: 10.1016/j.jnoncrysol.2006.02.108
30. Sinha A., Mahata T., Sharma B.P. (2002): Carbothermal route for preparation of boron carbide powder from boric acid–citric acid gel precursor. *Journal of Nuclear Materials*, *301*, 165–169. doi: 10.1016/S0022-3115(02)00704-3
31. Kakiage M., Tahara N., Yanase I., Kobayashi H. (2011): Low-temperature synthesis of boron carbide powder from condensed boric acid–glycerin product. *Materials Letters*, *65*, 1839-1841. doi: 10.1016/j.matlet.2011.03.046
32. Kakiage M. (2018): Low-temperature synthesis of boride powders by controlling microstructure in precursor using organic compounds. *Journal of the Ceramic Society of Japan*, *126*, 602-608. doi: 10.2109/jcersj2.18093
33. Pender M.J., Forsthoefel K.M., Sneddon L.G. (2003): Molecular and polymeric precursors to boron carbide nanofibers, nanocylinders, and nanoporous ceramics. *Pure and Applied Chemistry*, *75*, 1287–1294. doi: 10.1351/pac 200375091287
34. Tahara N., Kakiage M., Yanase I., Kobayashi H. (2013): Effect of addition of tartaric acid on synthesis of boron carbide powder from condensed boric acid–glycerin product. *Journal of Alloys and Compounds*, *573*, 58-64. doi: 10.1016/j.jallcom.2013.03.255
35. Chen X.W., Dong S.M., Kan Y.M., Zhou H.J., Hu J.B., Ding Y.S. (2016): Effect of glycerine addition on the synthesis of boron carbide from condensed boric acid–polyvinyl alcohol precursor. *RSC Advances*, *6*, 9338-9343. doi: 10.1039/C5RA23303H
36. Kakiage M., Tominaga Y., Yanase I., Kobayashi H. (2012): Synthesis of boron carbide powder in relation to composition and structural homogeneity of precursor using condensed boric acid–polyol product. *Powder Technology*, *221*, 257–263. doi: 10.1016/j.powtec.2012.01.010
37. Shawgi N., Li S.X., Wang S., Wang Z., Nie Y.N. (2017): Synthesis of nano particles and fiber-like shape boron carbide powder from ploy(vinyl alcohol) and boric acid. *Journal of Sol-Gel Science and Technology*, *82*, 450-457. doi: 10.1007/s10971-017-4320-4
38. Kakiage M., Tahara N., Yanagidani S., Yanase I., Kobayashi H. (2011): Effect of boron oxide/carbon arrangement of precursor derived from condensed polymer-boric acid product on low-temperature synthesis of boron carbide powder, *Journal of the Ceramic Society of Japan*, *119*, 422-425. doi: 10.2109/jcersj2.119.422
39. Najafi A., Golestani-Fard F., Rezaie H.R., Ehsani N. (2011): Effect of APC addition on precursors properties during synthesis of B_4C nano powder by a sol–gel process. *Journal of Alloys and Compounds*, *509*, 9164-9170. doi: 10.1016/j.jallcom.2011.06.103
40. Su W.-F. (2013). *Principles of polymer design and synthesis*. 1st ed. Springer.
41. Tang X., Alavi S. (2011): Recent advances in starch, polyvinyl alcohol based polymer blends, nanocomposites and their biodegradability. *Carbohydrate Polymers*, *85*, 7-16. doi: 10.1016/j.carbpol.2011.01.030
42. Finch C.A. (Ed.) (1992). *Polyvinyl alcohol-developments*. 2nd ed., John Wiley & Sons.
43. Chan L.W., Hao J.S., Heng P.W.S. (1999): Evaluation of permeability and mechanical properties of composite polyvinyl alcohol films. *Chemical and Pharmaceutical Bulletin*, *47*, 1412-1416. doi: 10.1248/cpb.47.1412
44. NPCS Board of Consultants&Engineers (2009). *The complete book on water soluble polymers*. 1st ed. Asia Pacific Business Press.
45. Balcı S., Sezgi N.A., Eren E. (2012): Boron oxide production kinetics using boric acid as raw material. *Industrial & Engineering Chemistry Research*, *51*, 11091−11096. doi: 10.1021/ie300685x
46. Yunlu K. (2016). *Bor bilesikleri, sentez yontemleri, ozellikleri, uygulamaları*. 1st ed. Boren Ulusal Bor Araştırma Enstıtusu.
47. Dias L.A.L., Alves W.A. (2019): Spectroscopic and conductometric behavior of boric acid in water and in an aprotic polar solvent. *Journal of Molecular Liquids*, *289*, 111152 1-5. doi: 10.1016/j.molliq.2019.111152
48. Yoon D.Y., Kim J.-C. (2016): Hydrophobically modified poly(vinyl alcohol) and boric acid-containing monoolein cubic phase as a glucose-responsive vehicle. *Colloids and Surfaces A: Physicochemical and Engineering Aspects*, *506*, 678-685. doi: 10.1016/j.colsurfa.2016.07.045
49. Fink J. (2015). *Water-based chemicals and technology for drilling, completion, and workover fluids*. 1st ed. Gulf Professional Publishing.
50. Woo J.Y., Shin E.J., Lee Y.H. (2010): Effect of boric acid treatment on the crystallinity and drawbility of poly(vinyl alcohol)-ıodinecomplexfilms.*PolymerBulletin*,*65*,169-180. doi: 10.1007/s00289-010-0279-9
51. Kakiage M., Tahara N., Tominaga Y., Yanagidani S., Yanase I., Kobayashi H. (2013): Effect of molecular structure of polyols with different molecular characteristics on synthesis of boron carbide powder. *Key Engineering Materials*, *534*, 61-65. doi: 10.4028/www.scientific.net/KEM.534.61
52. Li X., Lei M., Gao S., Yan S., Wang X., Xing P. (2019): Effect of initial compositions on boron carbide synthesis and corresponding growth mechanism. *Advances in Applied Ceramics Structural, Functional and Bioceramics*, *118*, 442–450. doi: 10.1080/17436753.2019.1664792